15th IFK
Proc. of the 15th International Fluid Power Conference <Symposium/Conference>
<DOI>

CFD-Based Optimization of a Supersonic Vacuum Ejector Using Combined 2D–3D Simulations and Latin Hypercube Sampling

Cong Liu*, Lennard Günther, Jürgen Weber

Chair of Fluid-Mechatronic Systems (Fluidtronics) – TUD Dresden University of Technology, Helmholtzstraße 7a, 01069 Dresden, Germany

E-Mail: cong.liu@tu-dresden.de

* *Corresponding Author*

Abstract.

This study proposes a combined two-dimensional (2D) and three-dimensional (3D) CFD-based optimization workflow with Latin Hypercube Sampling (LHS) for vacuum ejector nozzles operating in the supersonic flow regime. The reliability of the numerical framework is first established through detailed validation against experimental measurements under both open- and closed-suction operating conditions. The results demonstrate that the adopted CFD setup, boundary conditions, and the RNG k-ε turbulence model can accurately reproduce the measured ejector performance. The numerical simulations further provide detailed insights into the internal supersonic flow structures, including oblique shocks, shock reflections, and downstream shock trains.

Building on this validated CFD framework, the combined 2D–3D optimization workflow is applied, in which a 2D axisymmetric model is coupled with LHS to perform large-scale parametric screening of ejector geometries with enhanced suction performance. The most promising configurations identified from the 2D–LHS optimization are subsequently reconstructed and verified using full 3D simulations. The close agreement in predicted performance improvement between the 2D optimization results and the corresponding 3D validation confirms the reliability of the proposed workflow. Owing to its reduced computational cost and validated predictive accuracy, the methodology provides a practical and efficient design tool for the development of energy-efficient vacuum ejectors and is well suited for industrial applications.

Keywords. Vacuum ejector, Supersonic flow, CFD simulation, Turbulence modeling, RNG k-ε model, Axisymmetric model, Latin Hypercube Sampling (LHS), Optimization

1. INTRODUCTION

Vacuum ejectors are widely used for generating negative pressure in industrial automation and material handling, particularly in systems for gripping, holding, and transporting components.

To better understand and quantify the influence of ejector geometry on overall performance, Computational Fluid Dynamics (CFD) has been extensively applied. Several studies have reported that 3D CFD simulations can accurately reproduce the flow phenomena observed in Schlieren visualization experiments, confirming the capability of numerical models to capture shock-wave and pseudo-shock structures within ejector nozzles. Zhu and Jiang [1] demonstrated that experimentally observed shock trains can be accurately predicted by 3D simulations, while Chen et al. [2] confirmed close agreement between numerical reconstruction of the first shock wave and experimental data. Similar investigations on Laval nozzles showed that Large-Eddy Simulation (LES) achieves excellent consistency with Schlieren results, capturing multi-shock pseudo-shock systems and shock–boundary layer interactions [3].

Although 3D CFD simulations can provide highly accurate representations of ejector flow fields, their considerable computational expense makes them impractical for large-scale optimization studies and industrial applications. Consequently, an increasing number of publications have focused on two-dimensional (2D) CFD analyses as a more efficient alternative. Gagan et al. [4] and Schieder [5] demonstrated that 2D axisymmetric simulations can approximate 3D results with reasonable accuracy for most ejector configurations. More recently, Little et al. [6] compared 2D CFD predictions with Schlieren and shadowgraph visualization results for a large-scale air ejector and reported strong agreement between simulation and experimental observations under on-design operating conditions, confirming that 2D CFD can reliably capture key flow features and performance trends. These findings indicate that, while 3D modeling remains indispensable for resolving complex flow interactions, 2D CFD provides a validated and computationally efficient approach for ejector design and performance evaluation.

CFD-based optimization studies have identified several geometric parameters that strongly influence ejector performance. Wang et al. [7] found that the divergent angle and throat length of the primary nozzle are critical to the entrainment ratio, while Ruangtrakoon et al. [8] showed that the throat diameter and area ratio affect both entrainment capability and back pressure. Dong et al. [9] highlighted an optimal range of mixing chamber length for peak performance, and Wang et al. [10] demonstrated that 2D CFD can effectively guide design optimization before 3D validation. Building on this, Yann et al. [11] optimized three key geometries—the constant-pressure mixing chamber length, throat diameter, and constant-area mixing chamber length—under varying nozzle configurations, showing that the coupling between these dimensions and nozzle geometry plays a decisive role in shock structure and energy efficiency.

Building upon these previous efforts, the present study proposes an integrated methodology that combines 2D and 3D CFD simulations with Latin Hypercube Sampling (LHS) for efficient and accurate ejector optimization. The LHS method ensures uniform coverage of the parameter space with far fewer samples compared to conventional random sampling [12]. In this framework, the ejector geometry is parameterized so that each key geometric parameter can be systematically varied within a predefined range. Using the LHS method, multiple combinations of these structural parameters are generated, resulting in a large set of sample ejector configurations that comprehensively cover the multidimensional design space. The 2D model, established through appropriate geometric simplification, is applied to simulate each sample configuration under identical boundary conditions, allowing rapid evaluation of suction performance. The most promising configurations obtained from the 2D simulations are subsequently reconstructed as full 3D models under identical computational and boundary conditions, to quantify the performance improvement achieved through optimization. This combined CFD–LHS framework enables systematic and accelerated optimization of ejector geometry, providing both high computational efficiency and reliable performance enhancement.

2. MEASUREMENT

The vacuum ejector investigated in this study is the nozzle module of a compact industrial ejector supplied by a leading manufacturer of vacuum-handling technology. A custom-designed adapter was used to mount the ejector on the experimental test bench while preserving the original inlet, suction, and outlet flow paths and ensuring airtight connections.

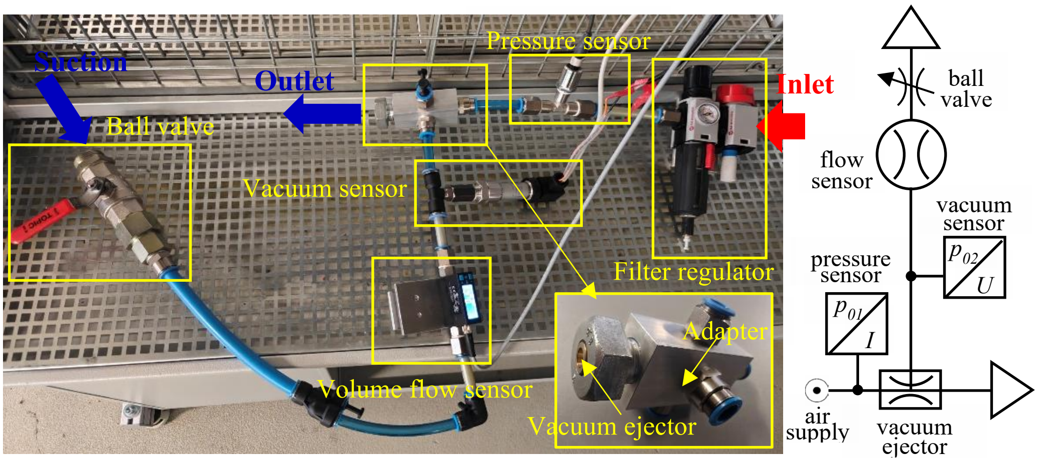

Figure 2.1 Experimental setup for vacuum ejector performance measurement with corresponding schematic diagram.

As shown in Figure 2.1, compressed air from the supply line passes through a filter–regulator unit and a pressure sensor before entering the motive nozzle as the primary flow. The inlet pressure p_{01} is measured upstream of the ejector, while the suction pressure p_{02} is recorded at the suction port using a vacuum sensor. The entrained air flow rate is monitored by a volume-flow sensor installed in the suction line.

A ball valve positioned between the flow sensor and the atmosphere allows adjustment of the suction-port boundary condition. With the valve open, ambient air is entrained into the ejector and the suction pressure can be continuously varied to represent different loading conditions (**open case**). When the valve is fully closed, the suction port is sealed and no air is entrained, corresponding to zero suction flow (**closed case**). This setup enables systematic characterization of ejector performance over a wide range of suction pressures and operating conditions. The experimental results are presented in Section 4 and compared with numerical simulations to evaluate the predictive accuracy of the CFD model.

3. CFD MODELING

Following the experimental measurements presented in the previous chapter, this section focuses on the numerical modeling of the ejector system. The modeling procedure begins with the governing conservation equations and the applied turbulence modeling approach, which together form the theoretical basis of the simulation framework. Subsequently, the 3D computational model is introduced, followed by a grid-independence study to ensure solution accuracy. To enhance computational efficiency, a 2D axisymmetric model is then developed as a simplified representation of the ejector geometry.

3.1. Fundamentals

3.1.1. Governing equations

The governing equations of the steady compressible flow inside the ejector are expressed in conservative form as follows. The mass conservation equation is given by

$$\frac{\partial(\rho u_i)}{\partial x_i} = 0 \ , \tag{3.1}$$

where ρ denotes the local fluid density, u_i the velocity component in the x_i direction.

The momentum conservation equation is written as

$$\frac{\partial(\rho u_i u_j)}{\partial x_j} = \rho f_i - \frac{\partial p}{\partial x_i} + \frac{\partial}{\partial x_j}\underbrace{\left[\mu\left(\frac{\partial u_j}{\partial x_i} + \frac{\partial u_i}{\partial x_j}\right) - \frac{2}{3}\mu\delta_{ij}\frac{\partial u_k}{\partial x_k}\right]}_{\tau_{ij}} \ , \tag{3.2}$$

where p represents the static pressure, f_i the body-force component per unit mass, and μ the dynamic viscosity of the working fluid; subscripts i, j and l denote Cartesian coordinates following the Einstein summation convention; δ_{ij} is the Kronecker delta and τ_{ij} the viscous stress tensor.

The energy conservation equation is expressed as

$$\frac{\partial}{\partial x_j}[u_i(\rho E + p)] = -\frac{\partial}{\partial x_i}\left(\sum_j h_j J_j\right) + S_h \ , \tag{3.3}$$

where E denotes the total energy per unit mass, h_j the specific enthalpy of the j^{th} species, $J_{j,i}$ the diffusive mass flux of species j in the x_i direction, and the S_h the volumetric energy source term accounting for additional heat transfer or dissipation effects.

3.1.2. Turbulence model

Accurate turbulence modeling is fundamental to the numerical prediction of high–Mach-number flows, making the selection of an appropriate turbulence model a critical component of the computational setup. Several studies have examined the applicability of different turbulence models for ejector flow simulations. Bartosiewicz et al. [11] conducted a comparative assessment of six turbulence closures for supersonic ejectors and reported that the RNG k-ε and SST k-ω models yielded the best agreement with experimental pressure distributions. Zhu et al. [13] performed a geometry-optimization study involving three turbulence models and found that the RNG k - ε formulation provided the closest correlation with the measured entrainment ratios. In a subsequent investigation, Zhu and Jiang [1] combined Schlieren visualization with three-dimensional CFD analysis and confirmed that the RNG k-ε model reproduced the shock-wave wavelength and mixing characteristics more accurately than other models. Collectively, these studies demonstrate that the RNG k-ε model delivers reliable and consistent performance in predicting the flow features of single-phase supersonic ejectors. Therefore, this turbulence model is adopted in the present work to describe the turbulent flow field within the vacuum ejector.

For compressible turbulent flows, the instantaneous velocity field is decomposed into mean and fluctuating components using Favre (density-weighted) averaging. Accordingly, the velocity components are expressed as [14]

$$u_i = \tilde{u}_i + u_i'', \quad \tilde{u}_i = \frac{\overline{\rho u_i}}{\bar{\rho}}, \quad \overline{\rho u_i''} = 0 \ , \tag{3.4}$$

where $\tilde{u}_i$ denotes the Favre-averaged velocity and u_i'' represents the corresponding density-weighted fluctuation.

Applying the Favre-averaging procedure to the compressible Navier–Stokes equations yields the Favre-averaged momentum equations, in which additional terms arise due to the turbulent velocity fluctuations. The resulting Favre-averaged momentum equation can be written as:

$$\frac{\partial(\bar{\rho}\tilde{u}_i\tilde{u}_j)}{\partial x_j} = \bar{\rho}\tilde{f}_i - \frac{\partial \bar{p}}{\partial x_i} + \frac{\partial \bar{\tau}_{ij}}{\partial x_j} + \frac{\partial}{\partial x_j}\underbrace{\left(-\bar{\rho}\widetilde{u_i''u_j''}\right)}_{R_{ij}} \tag{3.5}$$

In Eq. (3.5), the term $-\bar{\rho}\widetilde{u_i''u_j''}$ represents the Reynolds stress tensor, which accounts for the momentum transport induced by turbulent fluctuations. Since this term introduces additional unknowns, the system of equations requires closure through an appropriate turbulence model.

In the present study, the Boussinesq eddy-viscosity hypothesis is adopted to relate the Reynolds stresses to the mean strain-rate tensor. Under this assumption, the Reynolds stress tensor is defined as

$$R_{ij} = -\bar{\rho}\widetilde{u_i''u_j''} = \mu_t\left(\frac{\partial \tilde{u}_i}{\partial x_j} + \frac{\partial \tilde{u}_j}{\partial x_i}\right) - \frac{2}{3}\bar{\rho}k\delta_{ij} \ , \tag{3.6}$$

where μ_t is the turbulent viscosity and k the turbulent kinetic energy.

Based on the Reynolds-stress closure in Eq. (3.6), the production of turbulent kinetic energy due to mean velocity gradients, G_k, is defined as the contraction of the Reynolds stresses with the mean velocity gradients and is written as

$$G_k = R_{ij}\frac{\partial \tilde{u}_i}{\partial x_j} \ . \tag{3.6b}$$

To complete the turbulence closure, transport equations for the turbulent kinetic energy k and its dissipation rate ε are introduced. In this work, the Renormalization Group (RNG) k-ε model is employed, as it has been shown to provide reliable predictions for high-speed compressible flows with strong shock–turbulence interactions.

The steady Favre-averaged transport equation for the turbulent kinetic energy k, including compressibility effects, is given by

$$\frac{\partial(\bar{\rho}\tilde{u}_i k)}{\partial x_i} = \frac{\partial}{\partial x_j}\left(\bar{\mu}\frac{\partial k}{\partial x_j} + \frac{\mu_t}{\sigma_k}\frac{\partial k}{\partial x_j}\right) + G_k + G_b - \bar{\rho}\varepsilon - Y_M + S_k \ , \tag{3.7}$$

where G_k denotes represents the production of turbulent kinetic energy due to mean velocity gradients, G_b denotes the production due to buoyancy effects, and S_k is an optional user-defined source term. The term $Y_M = 2\bar{\rho}\epsilon M_t^2$ accounts for the additional dilatational dissipation arising from compressibility, following the model proposed by Sarkar (1991). The turbulent Mach number is defined as $M_t = \sqrt{2k}/a$, where a is the local speed of sound.

The corresponding transport equation for the dissipation rate ε is written as

$$\frac{\partial(\bar{\rho}\tilde{u}_i\varepsilon)}{\partial x_i} = \frac{\partial}{\partial x_j}\left(\bar{\mu}\frac{\partial \varepsilon}{\partial x_j} + \frac{\mu_t}{\sigma_\varepsilon}\frac{\partial \varepsilon}{\partial x_j}\right) + C_{1\varepsilon}\frac{\varepsilon}{k}(G_k + C_{3\varepsilon}G_b) - C_{2\varepsilon}\bar{\rho}\frac{\varepsilon^2}{k} - R_\varepsilon + S_\varepsilon \tag{3.8}$$

In this equation, $C_{1\varepsilon}$ and $C_{2\varepsilon}$ are model constants, G_k and G_b retain their definitions from the k-equation, and S_ε denotes a user-defined source term. The additional term R_ε is specific to the RNG formulation and represents a correction accounting for the interaction between turbulence dissipation and mean strain rate, which enhances the model's performance in rapidly strained and high-shear flows. All empirical constants adopt their default values as implemented in ANSYS Fluent 2024R2.

$$\sigma_k = 1.0,\ \sigma_\varepsilon = 1.3,\ C_{1\varepsilon} = 1.42,\ C_{2\varepsilon} = 1.68,\ C_\mu = 0.0845$$

3.1.3. Advanced numerical settings for supersonic simulation

Supersonic CFD simulations are prone to numerical instabilities caused by strong shock interactions and steep flow gradients. To ensure stable and convergent solutions, the High-Speed Numerics (**HSN**) scheme and the built-in Solution Steering strategy of the density-based implicit solver in ANSYS Fluent were employed. These approaches enhance numerical robustness in shock-dominated flows and improve convergence behavior [15].

3.2. 3D modeling

To ensure the accuracy of the numerical results, the 3D simulation model was developed based on the internal configuration of the vacuum ejector assembled with the adapter, as illustrated in Figure 3.1. The annular gap volume, originally present in the compact ejector design, was also reproduced in the model to accurately represent the real operating condition, in which suction occurs from a single direction toward the ejector.

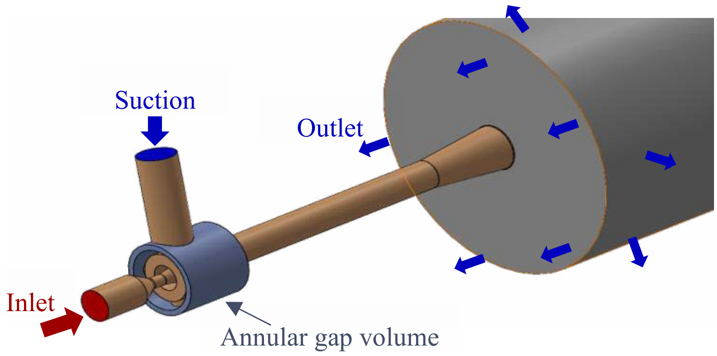

Figure 3.1 3D vacuum ejector model with annular gap volume

The computational domain was discretized using a poly-hexcore mesh generated in Fluent Meshing, as illustrated in Figure 3.2. This hybrid configuration combines structured hex-core regions with polyhedral transition zones, providing a good balance between mesh quality, numerical accuracy, and computational efficiency [16].

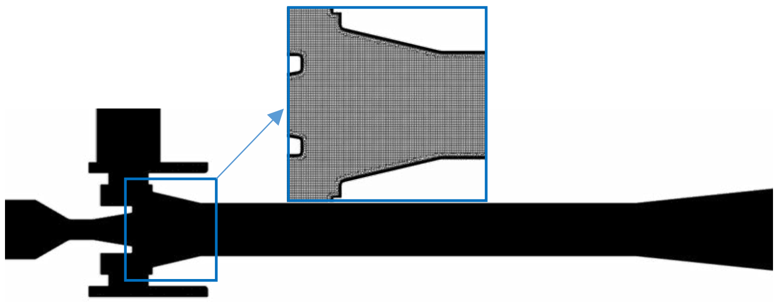

Figure 3.2 3D computational mesh of the vacuum ejector and detailed view

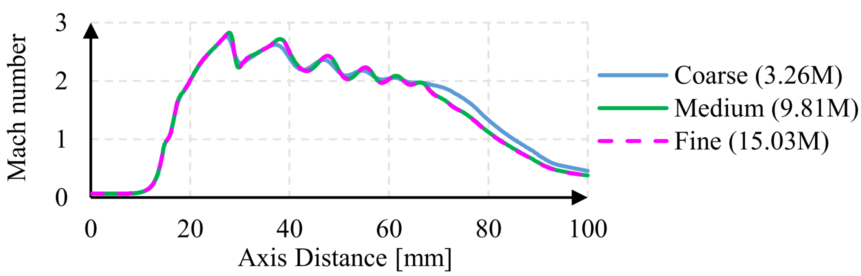

Figure 3.3 Comparison of Mach number distributions along the ejector centerline for different mesh resolutions

A grid independence study with three mesh resolutions was conducted to assess the influence of mesh density on simulation accuracy (Figure 3.3). The coarse, medium, and fine meshes contained approximately 3.26, 9.81, and 15.03 million cells, respectively. While the coarse mesh fails to adequately resolve the shock structures along the ejector centerline, the medium and fine meshes yield nearly identical Mach number distributions. Therefore, the medium mesh was selected for all subsequent simulations as an optimal compromise between numerical accuracy and computational cost.

3.3. Model reduction from 3D to 2D axisymmetric

Although three-dimensional CFD simulations yield highly accurate predictions of the ejector flow field, each case requires approximately five hours to complete on the TU Dresden high-performance computing (HPC) cluster (256 cores, Intel® Xeon® Platinum 8470). Consequently, such simulations are impractical for extensive parametric studies involving multiple geometric variations.

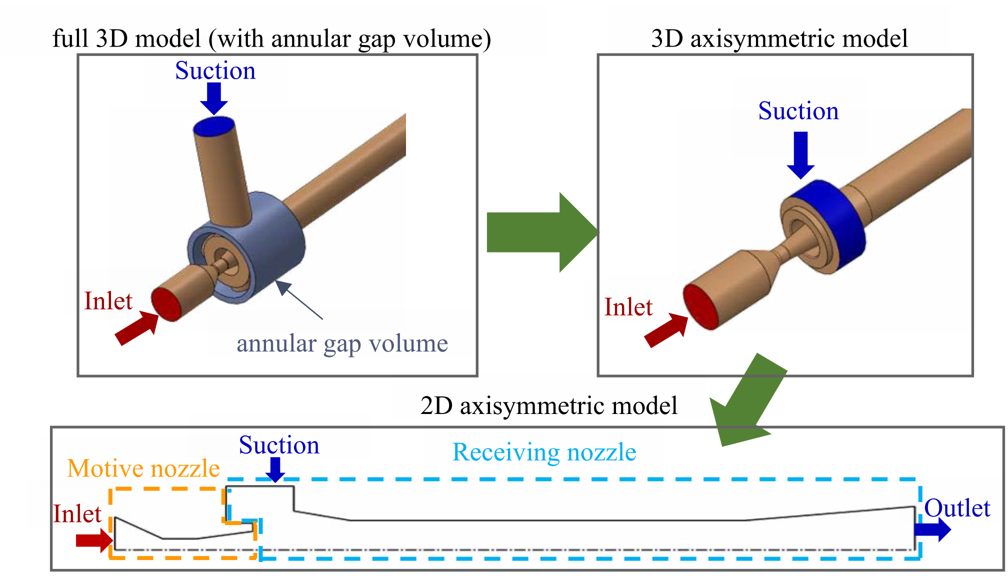

Figure 3.4 Transition from the 3D model to the simplified 2D axisymmetric model

To enhance computational efficiency, the model was progressively simplified, as illustrated in Figure 3.4. In the first step, the 3D ejector with the annular gap volume was reduced to a rotationally symmetric configuration, which preserves the main internal flow structures while omitting external domains. In the second step, this geometry was further simplified to a 2D axisymmetric model for parametric analysis.

In this process, it is important to note that the 2D axisymmetric simulations in ANSYS Fluent are solved in cylindrical coordinates, where all flow variables are expressed as functions of the radial and axial directions. Although the azimuthal (swirl) velocity component is neglected, previous validation work [5] has demonstrated that 2D axisymmetric formulations can still accurately capture the essential supersonic jet characteristics, including shock-wave structures and entrainment behavior. Therefore, 2D simulations provide a reliable and computationally efficient approach for modeling supersonic ejector flows, particularly during the preliminary optimization phase.

3.4. Boundary condition and numerical setup

To ensure that the numerical model accurately represents the experimental operating conditions, the boundary conditions and numerical settings of the three-dimensional (3D) CFD simulations are summarized in Table 1. Two operating modes were investigated: the open case, in which the inlet pressure was kept constant while the suction pressure was varied to represent different loading conditions, and the closed case, in which the suction port was sealed and defined as a wall boundary while the inlet pressure was varied.

Table 1 Overview of boundary conditions and simulation parameters

		Open case		Closed case	
		Type	Value	Type	Value
Boundary conditions	Inlet	Pressure inlet	4.8 bar	Pressure inlet	2.3…6 bar
	Suction	Pressure inlet	-210…-810 mbar	Wall	–
	Outlet	Pressure outlet	Atmosphere	Pressure outlet	Atmosphere
Numerical setup	Solver	Density-based			
	Formulation	Implicit			
	Turbulence model	RNG k-ε			
	Wall treatment	Standard wall function			
	Material	Air			

4. RESULTS AND DISCUSSION

The boundary conditions and numerical settings summarized in Table 1 were implemented to analyse the flow characteristics and performance of the vacuum ejector under both open- and closed-suction operating conditions. In this section, the predicted internal flow structures obtained from different CFD models are first compared, followed by a quantitative validation against experimental measurements. Based on these results, the applicability of simplified axisymmetric models is discussed.

4.1. *Flow-field comparison of different CFD models*

Figure 4.1 compares the Mach-number contours obtained from the full 3D model, the 3D axisymmetric model, and the 2D axisymmetric model under identical boundary conditions. All three simulations predict the formation of the first oblique shock at nearly the same axial location, with comparable inclination and strength. This close agreement indicates that the generation of the initial shock is predominantly governed by the motive-nozzle geometry and can be robustly captured by both three-dimensional and axisymmetric formulations.

Downstream of the first shock, noticeable differences emerge between the full 3D model and the two axisymmetric configurations. In the full 3D simulation, the suction flow enters the ejector through a geometrically asymmetric inlet connected to the annular gap volume, resulting in localized three-dimensional flow interactions that influence the subsequent development of the supersonic jet. In contrast, the axisymmetric models employ an idealized annular suction boundary, which leads to a more circumferentially uniform inflow and, consequently, a more symmetric Mach-number distribution within the ejector.

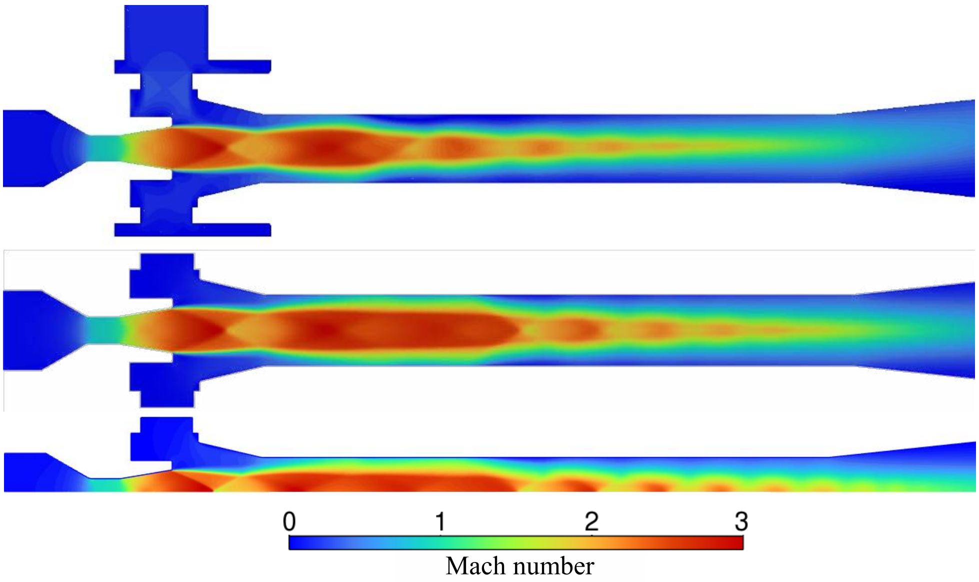

Figure 4.1 Mach-number contours of the full 3D (top), 3D axisymmetric (middle), and 2D axisymmetric (bottom) CFD simulations

When comparing the two axisymmetric simulations, the Mach-number distributions predicted by the 2D and 3D axisymmetric models are found to be qualitatively similar over most of the flow domain. Minor differences are mainly reflected in a smoother and less sharply defined shock train in the 2D solution, which can be attributed to the inherent limitations of the two-dimensional formulation, such as the inability to resolve three-dimensional effects including azimuthal velocity components, asymmetric mixing, and localized shock–turbulence interactions. Nevertheless, the overall expansion–compression pattern, shock spacing, and decay of the supersonic core remain consistent between the two axisymmetric models.

4.2. *Quantitative validation against experimental data*

The simulation results for both the open- (left) and closed-suction (right) cases within the operating range are presented in Figure 4.2. In this context, the vacuum level is defined as the pressure difference between the ambient atmospheric pressure and the absolute pressure measured near the suction port, i.e., Vacuum $= p_{atm} - p_{abs}$.

For the full 3D model, the predicted suction volumetric flow rates under open-suction conditions show excellent agreement with the experimental measurements. A similarly close correspondence is observed for the vacuum level under closed-suction conditions. This consistency across both operating modes demonstrates the validity of the applied boundary conditions, numerical setup, and turbulence modeling strategy, confirming that the adopted CFD framework can accurately reproduce the ejector performance.

The simplified 3D axisymmetric and 2D axisymmetric models successfully capture the overall performance trends of the ejector but predict slightly higher suction volumetric flow rates under open-suction conditions. As discussed in Section 3.3 and illustrated in Figure 3.4, this deviation arises from the geometric simplification of the suction region. In the axisymmetric configurations, the suction boundary is represented as an idealized annular surface, which effectively enlarges the area available for entrained air compared with the asymmetric suction inlet of the full 3D model. This enlarged entrainment area facilitates a greater inflow of secondary air and consequently leads to an overprediction of the suction flow rate in the open-suction case.

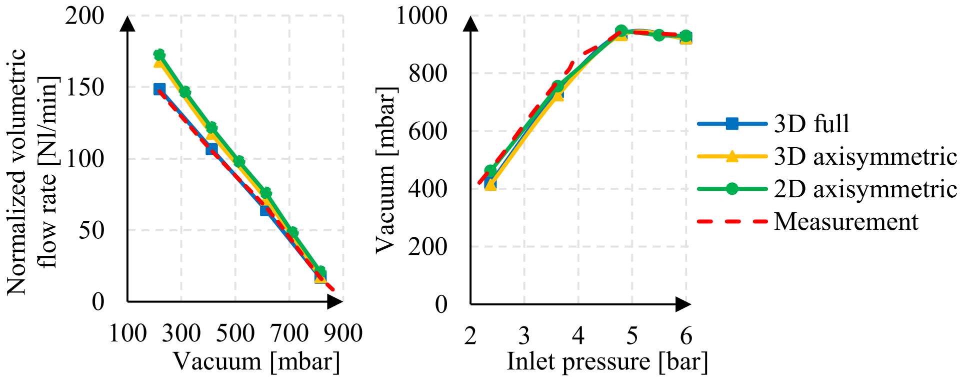

Figure 4.2 Comparison of experimental and simulation results for the open (left) and closed (right) suction cases using different CFD models

Under closed-suction conditions, however, the differences between the three models become negligible. Since the suction port is defined as a wall boundary and no external air is entrained, the internal flow field is no longer influenced by the suction boundary geometry. Instead, the ejector performance is primarily governed by the expansion, shock formation, and recompression processes of the motive jet. As a result, all three modeling approaches yield nearly identical predictions of the vacuum level.

4.3. Discussion and implications for model reduction

Taken together, the qualitative flow-field comparison and the quantitative validation against experimental data demonstrate that the dominant supersonic flow features and overall ejector performance are consistently captured by the axisymmetric formulations. While the full 3D model provides the most detailed representation of the internal flow field, the close agreement between the 2D and 3D axisymmetric results indicates that, once axisymmetry is assumed, the additional dimensional reduction introduces only limited deviations in the predicted flow field.

This finding supports the use of the 2D axisymmetric model for large-scale parametric simulations and preliminary geometry screening, where computational efficiency is essential and the primary interest lies in comparative performance trends rather than in detailed three-dimensional flow structures.

5. EJECTOR OPTIMIZATION WITH LATIN HYPER CUBE SAMPLING

In the present study, the optimization is conducted primarily under open-suction operating conditions, as this case directly reflects the ejector performance relevant to energy efficiency during practical operation. As stated in [17], the geometric parameters of a vacuum ejector strongly interact with one another, and it is therefore more meaningful to vary the key parameters simultaneously rather than individually. The vacuum ejector is parameterized as illustrated in Figure 5.1, and its geometry is defined by several characteristic dimensions that determine the internal flow passages.

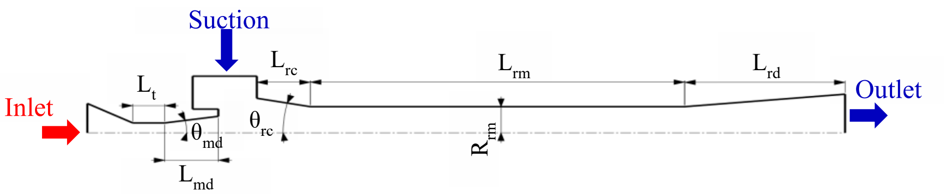

Figure 5.1 Parameterized geometry of the vacuum ejector

Based on previous studies, the throat section of the motive nozzle plays a crucial role in compressing and accelerating the primary flow to Mach number M=1 [18][19]. Variations of the throat radius R_t significantly affect the mass flow rate of the induced secondary stream and, consequently, alter the overall operating range of the ejector. Furthermore, changing R_t would require substantial modifications to both the motive and receiving nozzle geometries, thus reducing the comparability between the optimized and reference geometries. For this reason, R_t was not considered as a design variable in the present optimization. This approach also reflects the practice in commercial compact ejector product lines, where different models are primarily distinguished by their inlet mass-flow capacities rather than by variations in the throat size.

The definitions of the geometric parameters and their respective variation ranges are summarized in Table 2.

Using the LHS method, a total of **1500** sample geometries were generated based on the parameter ranges listed in Table 2. The sample size was selected to ensure sufficient coverage of the high-dimensional parameter space while maintaining a feasible computational cost [20].

Since the primary objective of the present study is the enhancement of energy efficiency, the optimization process was conducted with a clear emphasis on the open-suction operating condition, which accounts for approximately 80% of the overall performance weighting. The closed-suction case was incorporated as a secondary criterion (20%) to ensure that the optimized geometries still maintain an acceptable vacuum level.

In the first selection stage, all geometries exhibiting a higher suction volumetric flow rate than the reference ejector under open-suction conditions were retained as candidate geometries. Because the throat radius R_t was kept constant, the primary mass flow rate at a given operating point remained nearly identical across all simulations, allowing direct comparison of the normalized suction volumetric flow rate without additional correction.

Table 2 Definition and variation ranges of the geometric parameters

Parameter	Description	Variation range
R_t	Throat radius of the motive nozzle	-
L_t	Length of the motive nozzle throat section	-45% ... 750%
L_{md}	Length of diverge section of motive nozzle	-75% ... 150%
θ_{md}	Angle of diverge section of motive nozzle	-85% ... 235%
θ_{rc}	Angle of converged section of receiving nozzle	-85% ... 165%
L_{rc}	Length of converged section of receiving nozzle	-15% ... 470%
R_{rm}	Radius of mixing chamber	-5% ... 25%
L_{rm}	Length of mixing chamber	-35% ... 160%
L_{rd}	Length of diverge section of receiving nozzle	-20% ... 380%

In the second stage, the retained candidate geometries were further evaluated under closed-suction conditions. A weighted performance metric combining the improvements in open- and closed-suction cases was then applied to rank the candidate geometries. Based on this weighted evaluation, two optimized ejector geometries, denoted as **Opti1** and **Opti2**, were selected for detailed comparison.

The simulated performance of the optimized ejector geometries under both open- and closed-suction conditions is presented in Figure 5.2. The relative improvements are evaluated with respect to their corresponding reference configurations: the 2D results are normalized by the baseline 2D axisymmetric model shown in Figure 4.2, while the 3D results are referenced to the baseline full 3D model simulations. This consistent benchmarking strategy ensures that the optimization outcomes are assessed within the same modeling framework and avoids cross-dimensional bias.

In the open-suction case, the 2D axisymmetric and full 3D models exhibit highly consistent improvement trends across the investigated operating range. Both optimized geometries show similar relative gains in suction volumetric flow rate, and the agreement between the 2D-based predictions and their 3D validation results is particularly pronounced. This strong correspondence confirms that the adopted optimization strategy—screening candidate geometries using computationally efficient 2D simulations and subsequently validating the most promising designs with full 3D models—is both reliable and effective. Moreover, it demonstrates that two-dimensional simulations are capable of capturing the dominant performance trends relevant to energy-efficiency enhancement.

Under closed-suction conditions, although the quantitative improvements predicted by the 2D and 3D models differ slightly, the overall trends remain consistent. An important observation from the right-hand plot of Figure 5.2 is that enhanced suction performance under open-suction conditions is accompanied by a reduction in the achievable vacuum level under closed-suction operation. This behavior indicates an inherent trade-off between maximizing energy-efficient suction capacity and attaining high vacuum levels, suggesting that these two objectives cannot be simultaneously optimized within a single ejector geometry.

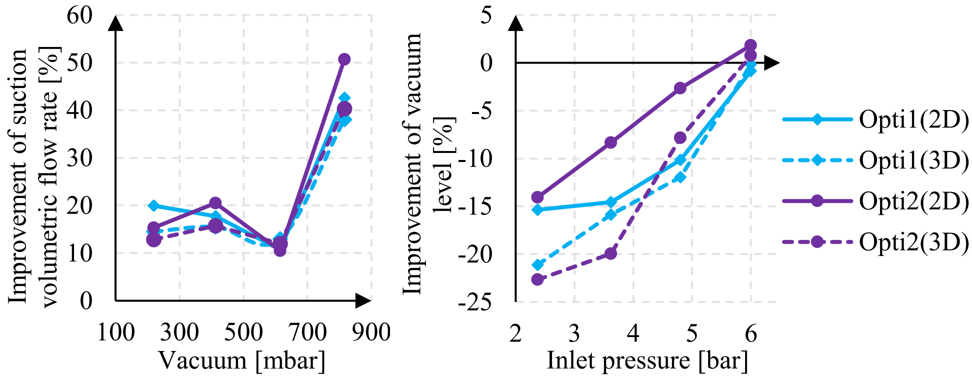

Figure 5.2 Improvement of the optimized ejector geometries under open- (left) and closed-suction (right) conditions

6. CONCLUSION

This study has demonstrated the accuracy and practical feasibility of an integrated CFD-based optimization methodology for vacuum ejector nozzles operating in the supersonic flow regime. By systematically combining experimental measurements with three-dimensional and two-dimensional numerical simulations, the reliability of the adopted CFD setup was established across both open- and closed-suction operating conditions. In particular, the RNG k-ε turbulence model was shown to accurately predict the suction volumetric flow rate in the open-suction case as well as the achievable vacuum level under closed-suction conditions, confirming its suitability for modeling supersonic ejector flows.

A key outcome of this work is the validation of a computationally efficient optimization framework that integrates 2D axisymmetric simulations with Latin Hypercube Sampling

(LHS) for large-scale parameter screening, followed by targeted full 3D model validation. The strong agreement observed between the optimization trends obtained from the 2D simulations and their corresponding 3D validation results demonstrates that the proposed workflow provides a reliable basis for identifying energy-efficient ejector geometries while significantly reducing computational cost. This confirms that simplified axisymmetric models, when properly validated, can be effectively employed in early-stage design and optimization of supersonic flow components.

The optimization results further reveal an inherent trade-off between maximizing suction capacity and achieving high vacuum levels, indicating that these performance objectives cannot be simultaneously optimized within a single ejector configuration. Consequently, the design of high-performance vacuum ejectors requires a balanced consideration of energy efficiency and attainable vacuum level, depending on the intended application.

Future work will extend the present methodology beyond numerical optimization by manufacturing and experimentally testing the optimized geometries to assess their real-world performance. Moreover, the proposed CFD–LHS framework is inherently applicable to a broad class of fluid-dynamic optimization problems in which the geometry can be parameterized and globally optimal configurations are sought. This includes, but is not limited to, ejector designs and other complex flow devices, where robust global exploration of the design space is required under strongly nonlinear flow conditions.

7. REFERENCES

[1] P. Jiang, Z. Zhu, "Experimental and numerical investigation of the effect of shock wave characteristics on the ejector performance," Energy Conversion and Management, vol. 86, pp. 233–241, 2014.

[2] W. Chen, Y. Hou, J. Zheng, D. Chong, and J. Yan, "Studies on shock wave structures in supersonic ejector and its influence on ejector performance," Heat Transfer Engineering, vol. 45, no. 7–8, pp. 631–641, 2024. DOI: 10.1080/01457632.2023.2213995

[3] C. Stemmer and S. Hickel, "Large Eddy Simulation of a Pseudo-Shock System within a Laval Nozzle," Gauss Centre for Supercomputing e.V., Technische Universität München, December 2021. Available: https://www.gauss-centre.eu/results/computational-and-scientific-engineering/large-eddy-simulation-of-a-pseudo-shock-system-within-a-laval-nozzle

[4] B. Gagan, M. Wójcik, W. Nowak, "Comparative study of turbulence models in application to gas ejectors," Energy Conversion and Management, vol. 77, pp. 137–145, 2014.

[5] M. Schieder, "Characterization and Optimization of Ejectors using Numerical Fluid Dynamics," Diploma Thesis, TU Wien, Vienna, Austria, Jan. 2023.

[6] A.B. Little, Y. Bartosiewicz, S. Garimella, "Visualization and Validation of Ejector Flow Field With Computational and First-Principles Analysis," J. Fluids Eng., Vol. 137, No. 5, 2015, Paper 051107. DOI: 10.1115/1.4029534.

[7] L. Wang, J. Yan, C. Wang, X. Li, "Numerical study on optimization of ejector primary nozzle geometries," International Journal of Refrigeration, vol. 76, pp. 219–229, 2017.

[8] N. Ruangtrakoon, T. Thongtip, S. Aphornratana, T. Sriveerakul, "CFD simulation on the effect of primary nozzle geometries for a steam ejector in refrigeration cycle," International Journal of Thermal Sciences, vol. 63, pp. 133–145, 2013.

[9] J. Dong, Q. Hu, M. Yu, W. Cui, D. Liang, H. Ma, X. Pan, "Numerical investigation on the influence of mixing chamber length on steam ejector performance," Applied Thermal Engineering, vol. 174, pp. 115204, 2020.

[10] L. Wang, M. Becker, S. Schneider, "Development of an ejector for passive hydrogen recirculation in PEM fuel cell systems by applying 2D CFD simulation," International Journal of Hydrogen Energy, vol. 44, no. 32, pp. 17564–17574, 2019.

[11] Y. Bartosiewicz, P. Desevaux, Z. Aidoun, and Y. Mercadier, "CFD–experiments integration in the evaluation of six turbulence models for supersonic ejector modeling," Proceedings of the International Conference on Ejectors and Applications (ICEA), 2004. https://api.semanticscholar.org/CorpusID:41016682.

[12] E.J. Pebesma, G.B.M. Heuvelink, "Latin hypercube sampling of Gaussian random fields," Technometrics, Vol. 41, No. 4, pp. 303–312, 1999.

[13] Y. Zhu, W. Cai, C. Wen, Y. Li, Numerical investigation of geometry parameters for design of high performance ejectors, Appl. Therm. Eng. 29 (2009) 898–905.

[14] ANSYS® Fluent Theory Guide, Release 2024 R2, ANSYS, Inc., Canonsburg, PA, USA, 2024.

[15] ANSYS® Fluent User's Guide, Release 2024 R2, ANSYS, Inc., Canonsburg, PA, USA, 2024.

[16] A. Wróblewski, A. Macek, A. Banasiewicz, and J. Wodecki, "Comparison of Hexcore and Poly-Hexcore computational meshes in the aspect of air flow modeling based on the actual geometry of mining excavations," IOP Conference Series: Earth and Environmental Science, vol. 1295, 012007, 2024. DOI: 10.1088/1755-1315/1295/1/012007

[17] J. Yan, R. Li, and C. Wang, "Optimization of Three Key Geometries of a Steam Ejector under Varied Primary Nozzle Geometries," Entropy, vol. 25, no. 1, p. 15, 2023. DOI: 10.3390/e25010015

[18] N. Gebhardt and J. Weber (Eds.), Hydraulik – Fluid-Mechatronik: Grundlagen, Komponenten, Systeme, Messtechnik und virtuelles Engineering, 7th ed., Springer Vieweg, Berlin/Heidelberg, Germany, 2020.

[19] G. N. Abramowitsch, Angewandte Gasdynamik, VEB Verlag Technik, Berlin, 1958.

[20] M. L. Stein, "Large sample properties of simulations using Latin hypercube sampling," Technometrics, vol. 29, no. 2, pp. 143–151, 1987. DOI: 10.1080/00401706.1987.10488205

8. ACKNOWLEDGEMENT

This research was funded by the Federal Ministry for Economic Affairs and Energy (BMWK), grant number 03EN4087B (EnerVaz: Design and development of innovative pneumatic vacuum generators with improved efficiency and reduced noise emission).

The authors gratefully acknowledge the Center for Information Services and High Performance Computing (ZIH) at Dresden University of Technology (TU Dresden) for providing the computational resources used in this work.

Biographies

Cong Liu received his diploma in Diploma in Mechanical Engineering in the fields of numerical multi-phase flow simulations of cavitation from TU Dresden in 2022. Since 2023 he is working as Research Associate at the Chair of Fluid-Mechatronic Systems (Fluidtronics), Institute of Mechatronic Engineering, Technische Universität Dresden. His research areas include numerical simulation and optimization of pneumatic and hydraulic systems, with a focus on CFD-based analysis and design improvement of flow components in industrial applications.

Lennard Günther received his diploma in Diploma in Mechanical Engineering in the fields of numerical multi-phase flow simulations of cavitation from TU Dresden in 2020. Since 2020 he is working as Research Associate at the Chair of Fluid-Mechatronic Systems (Fluidtronics), Institute of Mechatronic Engineering, Technische Universität Dresden. His research areas include valve development in the field of industrial applications as well as research and numerical investigations of special internal flow phenomena of hydraulic components.

Jürgen Weber has been appointed in 2010 as a University Professor and the Chair of Fluid-Mechatronic Systems as well as the Director of the Institute of Fluid Power at the TUD Dresden University of Technology, Germany, and took on the leadership of Institute of Mechatronic Engineering in 2018. He finished his doctorate in 1991 and was an active Senior Engineer at the former Chair of Hydraulics and Pneumatics until 1997. This was followed by a 13-year industrial phase. Besides his occupation as the Head of the Department Hydraulics and Design Manager for Mobile and Tracked Excavators, starting in 2002, he took on responsibility for the hydraulics in construction machinery at CNH worldwide. From 2006 onwards, he was the Global Head of Architecture for hydraulic drive and control systems, system integration and advance development CNH construction machinery.